Observation of an Electron Microburst With an Inverse Time-of-Flight Energy Dispersion

M. Shumko[1,2,3], Y. Miyoshi[4], L.W. Blum[5], A.J. Halford[2], A.W. Breneman[2], A.T. Johnson[6], J.G. Sample[7], D.M. Klumpar[7], and H.E. Spence[6]

[1]Johns Hopkins University Applied Physics Laboratory, Laurel, Maryland, USA
[2]NASA's Goddard Space Flight Center, Greenbelt, Maryland, USA
[3]Department of Astronomy, University of Maryland, College Park, Maryland, USA
[4]Institute for Space-Earth Environmental Research, Nagoya University, Japan
[5]Laboratory for Atmospheric and Space Physics, University of Colorado, Boulder, Colorado, USA
[6]Institute for the Study of Earth, Oceans, and Space, University of New Hampshire, New Hampshire, USA
[7]Department of Physics, Montana State University, Bozeman, Montana, USA

Key Points:

- FIREBIRD-II observed a microburst whose 250 keV electrons arrived before the 650 keV electrons
- We estimate that the observed inverse energy dispersion of 0.1 ms/keV is statistically significant
- Our observations are consistent with the inverse time-of-flight model of chorus waves resonating with 100s keV electrons

Corresponding author: M. Shumko, `msshumko@gmail.com`

Abstract

Interactions between whistler mode chorus waves and electrons are a dominant mechanism for particle acceleration and loss in the outer radiation belt. One form of this loss is electron microburst precipitation: a sub-second intense burst of electrons. Despite previous investigations, details regarding the microburst-chorus scattering mechanism—such as dominant resonance harmonic—are largely unconstrained. One way to observationally probe this is via the time-of-flight energy dispersion. If a single cyclotron resonance is dominant, then higher energy electrons will resonate at higher magnetic latitudes: sometimes resulting in an inverse time-of-flight dispersion with lower-energy electrons leading. Here we present a clear example of this phenomena, observed by a FIREBIRD-II CubeSat on 27 August 2015, that shows good agreement with the Miyoshi-Saito time-of-flight model. When constrained by this observation, the Miyoshi-Saito model predicts that a relatively narrowband chorus wave with a ~ 0.2 of the equatorial electron gyrofrequency scattered the microburst.

Plain Language Summary

Wave-particle interactions are a ubiquitous phenomenon in plasmas. Around Earth, interactions between electrons and a plasma wave termed whistler mode chorus leads to both the acceleration of the outer Van Allen radiation belt electrons, and rapid precipitation of electrons into Earth's atmosphere. One form of this precipitation is called electron microbursts: a sub-second and intense bursts of electrons most often observed by high altitude balloons and low Earth orbiting satellites. While microbursts have been studied since the dawn of the Space Age, fundamental details regarding how they are generated are largely unknown. One clue to the properties of the scattering mechanism comes from energy-dependent time-of-flight dispersion signatures. Electrons with a larger kinetic energy move faster, and will therefore precipitate before the electrons with lower kinetic energy. However, in this paper we show observations made by the FIREBIRD-II CubeSat mission of the opposite: lower-energy electrons arriving first. This counter-intuitive phenomena, termed inverse time-of-flight energy dispersion, together with models, is a powerful tool to sense the detailed nature of how plasma waves scatter electrons in Earth's near space environment.

1 Introduction

Wave-particle interactions are ubiquitous phenomena in plasmas and are a vitally important driver of Earth's outer Van Allen radiation belt dynamics. Specifically, whistler mode chorus waves are believed to contribute significantly to radiation belt electron acceleration and loss (e.g., Miyoshi et al., 2003; Bortnik & Thorne, 2007; Miyoshi et al., 2013; Reeves et al., 2013; Lejosne et al., 2022). Whistler mode chorus waves are right-hand circularly polarized and exist in two frequency bands: the lower band spanning approximately $\Omega = 0.1 - 0.4\ \omega_{ce}$, and the upper band approximately spanning $\Omega = 0.5 - 0.9\ \omega_{ce}$ with a gap near $0.5\ \omega_{ce}$, where ω_{ce} is the electron gyro frequency (J. Li et al., 2019). Chorus waves often originate at the magnetic equator and propagate to higher magnetic latitudes (λ) where they can scatter electrons over a wide range of energies (e.g. Horne & Thorne, 2003).

The effect of a chorus wave on an electron will, in general, differ in each subsequent gyration and will average to zero over many gyrations (Walker, 1993). However, if the electron experiences a static electric field during its gyration, the electron is in resonance and can experience substantial acceleration or deceleration (e.g. Omura et al., 2009). One form of chorus-electron gyro-resonance that leads to significant microburst flux occurs when the electrons and the chorus wave are counter-steaming (e.g., Tsurutani & Lakhina, 1997; Lorentzen et al., 2001; Miyoshi et al., 2020; Kang et al., 2022). The resonance condition between relativistic electrons and field aligned chorus waves is often expressed as
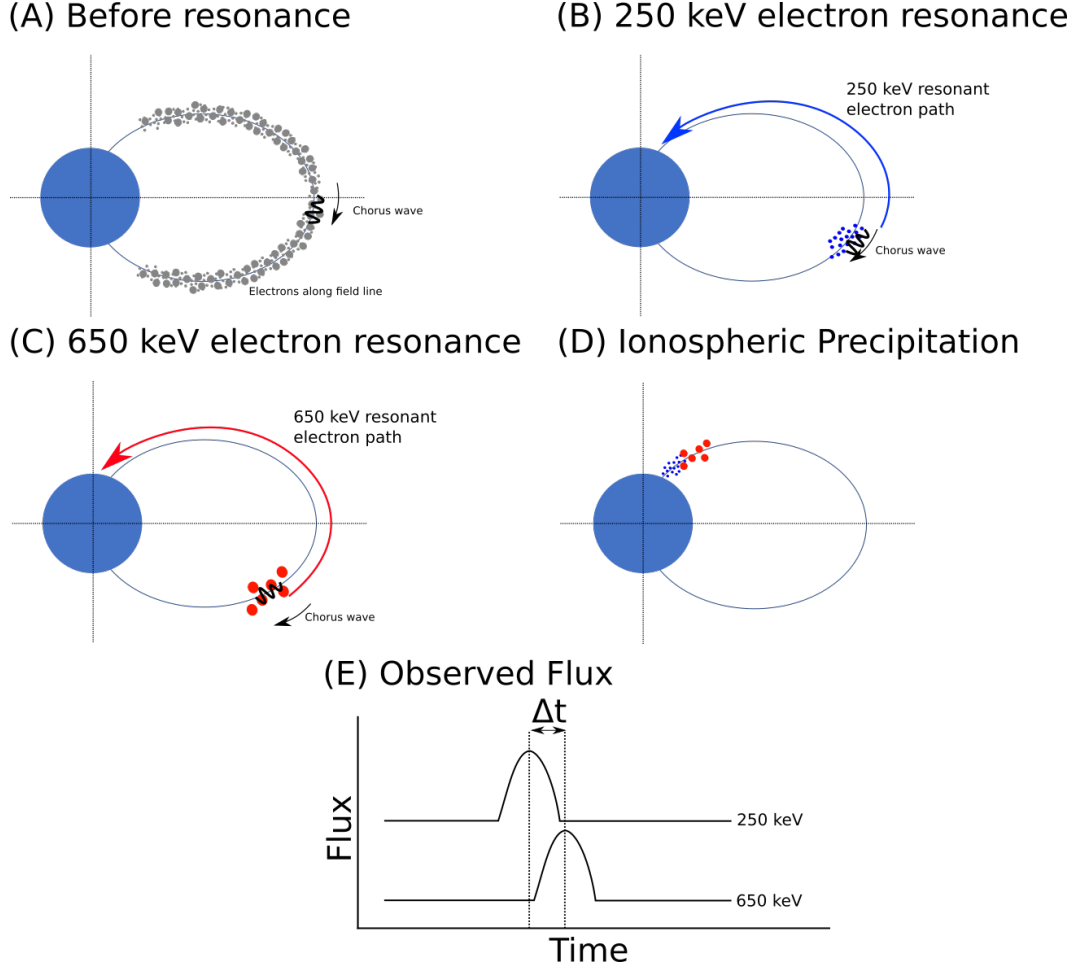
$$\Omega + k_{||}v_{||} = \frac{n\omega_{ce}}{\gamma}, \tag{1}$$

where the wave vector parallel to the background magnetic field is $k_{||}$, the electron velocity parallel to the background magnetic field is $v_{||}$, the resonance harmonic is n, and the Lorentz factor is γ. Here we use the sign convention where $k_{||}$ and $v_{||}$ are both positive, despite the fact that they must counter-propagate for resonance to occur.

Lorentzen et al. (2001) applied this resonance condition to estimate the energy-dependent magnetic latitude of electrons interacting with chorus waves. The authors found that parallel chorus waves can scatter 1 MeV electrons into the atmosphere via the $n = 1$ cyclotron resonance harmonic at high magnetic latitudes ($\lambda = 15°-30°$). Horne and Thorne (2003), Miyoshi et al. (2020), A. V. Artemyev et al. (2021), and others came to a similar conclusion. Alternatively, oblique chorus waves can scatter electrons too, but that necessitates higher n (or $n = 0$ Landau resonance) and intense waves that are seldom observed (e.g. A. Artemyev et al., 2016; Agapitov et al., 2018; A. Artemyev et al., 2022). Out of the two possibilities, recent theoretical and observational results favor the cyclotron resonance of field-aligned chorus waves with electrons (e.g. Shen et al., 2021; Chen et al., 2022); this is the assumption that we adopt here.

Assuming field-aligned chorus waves, the $n = 1$ resonance condition results in a energy-dependent electron time-of-flight (TOF) dispersion that has been modeled in a few studies (e.g. Miyoshi et al., 2010; Saito et al., 2012). With prescribed wave parameters, these TOF models predict microburst precipitation time as a function of energy (dispersion curves). In other words, observations of the TOF energy dispersion, together with models, can constrain the high-altitude wave environment that produces the precipitation. Miyoshi et al. (2010) developed a TOF model by considering the magnetic latitude where the first order cyclotron resonance condition is satisfied. The TOF ingredients include the time it takes the chorus wave to propagate to the λ where it will resonate with counter-propagating electrons, the time the recently-resonant electron take to reach the magnetic equator, and the quarter bounce period for the electron to travel from the magnetic equator to the ionosphere. The authors used this model to describe the observed energy dispersion of $1-10$ keV electrons: the higher energy electrons arrive *before* the lower energy electrons. In passing, Miyoshi et al. (2010) also mentioned that their TOF model sometimes predicted inverse dispersion: the higher energy electrons arrive *after* the lower energy electrons—a counterintuitive effect of interest in this study.

Saito et al. (2012) used this TOF model to further explore the necessary conditions for inverse dispersed microbursts. The authors found that the TOF dispersion should be normal (high energy electrons lead) for sub-100 keV electrons, and inverse for > 100 keV electrons. This effect was also confirmed with test-particle simulations in Miyoshi et al. (2020) and Chen et al. (2020). We illustrate how this model can produce inverse dispersion in Fig. 1(A)-(D). An instrument with sufficient time and energy resolution, as well as sufficient energy extent, would observe a bow-shaped TOF dispersion curve spanning 10-1000 keV energies. Considering a particle instrument sensitive to > 200 keV electrons, the TOF model predicts that that those electrons will be inverse dispersed. Figure 1(E) shows how this dispersion would appear in a time series.

A note regarding the terminology used in Saito et al. (2012). Saito et al. (2012) use the *negative* and *positive* dispersion terminology (in reference to the slope of the peak microburst flux in an energy-time spectrogram). For clarity, Saito et al. (2012)'s *positive* dispersion is equivalent to Miyoshi et al. (2010)'s *inverse* dispersion. And for simplicity, we henceforth use the *inverse* dispersion nomenclature only.

(A) Before resonance

250 keV resonant electron path

(B) 250 keV electron resonance

Chorus wave

Electrons along field line

(C) 650 keV electron resonance

650 keV resonant electron path

Chorus wave

(D) Ionospheric Precipitation

(E) Observed Flux

Δt

Flux

250 keV

650 keV

Time

Figure 1. The time progression of electrons undergoing counter-streaming cyclotron resonance with field-aligned chorus wave. Panel (A) shows the electrons along the field line and a chorus wave as it begins propagating. Panels (B) and (C) show the magnetic latitudes where 250 and 650 keV counter-streaming electrons resonate with the chorus wave, and their path to the ionosphere. The 250 keV electrons resonate first, followed by the 650 keV electrons shorty after. While faster, the higher energy electrons resonate later, and must travel further to the ionosphere (represented by the curved arrows of differing length). Panel (D) shows the locations of these two microburst electron populations at the end of the their propagation in the ionosphere—the high energy electrons lag slightly behind the low energy electrons. At the same time as Panel (D), Panel (E) shows the observed flux in low Earth orbit. Here, the low-energy microburst peak arrives Δt before the high-energy microburst peak.

The TOF model allows us to constrain the chorus wave frequencies, range of resonant λ, and test if (or when) the $n = 1$ cyclotron resonance assumption—common in wave-particle scattering models—is valid.

While normally dispersed electron precipitation have been reported elsewhere, especially in relation to pulsating aurora (e.g. Yau et al., 1981; Sato et al., 2004; Miyoshi et al., 2010; Kawamura et al., 2021), inverse dispersed microbursts have not been clearly observed. In this study we use The Focused Investigations of Relativistic Electron Burst Intensity, Range, and Dynamics (FIREBIRD-II; Crew et al. (2016); Johnson et al. (2020)) CubeSats and show a clear example of an inverse dispersed microburst observed on 27 August 2015 at 12:40:37 UT. The 18.75 ms cadence data was sufficient to resolve the dispersion in four energy channels spanning $230-770$ keV. We fit the observed dispersion with a line and use Bayesian inference to account for instrument uncertainties. Lastly, we place our observations in context by constraining the wave-particle interaction using the TOF model (Miyoshi et al., 2010; Saito et al., 2012).

2 Methodology

2.1 The FIREBIRD-II CubeSats

The FIREBIRD-II mission consists of a pair of 1.5U CubeSats launched on 31 January 2015 into a polar low Earth orbit. Part of their mission was to use their small spatial separation to quantify the spatial scale size of 200 keV to > 1 MeV microbursts with the collimated detector's 6 energy channels (Crew et al., 2016; Shumko et al., 2018). After a few months, their separation increased beyond the size of any known microburst (a few hundred km, see Shumko, Johnson, Sample, et al. (2020) and references within), and the FIREBIRD-II science team began pursuing secondary science objectives including coordinated observations during conjunction with high altitude satellites (Breneman et al., 2017; Capannolo et al., 2019; Duderstadt et al., 2021), and high time resolution campaigns to observe microburst dispersion. For the latter objective, FIREBIRD-II collected 18.75 and 12.50 ms high resolution (HiRes) data—a cadence on the order of the inverse dispersion delays theorized by Saito et al. (2012) for electron precipitation in the 100s keV range.

2.2 Microburst Identification and Fitting

Finding and analyzing inverse-dispersed microbursts consists of three main steps: find microbursts, calculate the time of the microburst peak as a function of energy, and quantify the TOF energy dispersion. These steps are expanded on below.

Step 1: we find microbursts in the FIREBIRD-II collimated detector data using the burst parameter algorithm (O'Brien et al., 2003) that has been used in numerous studies (e.g. Douma et al., 2017; Shumko et al., 2021). To use this detection algorithm, we calculated the 100 and 500 ms running average counts in the ~ 250 keV channel (lowest energy channel). To the averaged counts we then applied the detection algorithm with the same parameters as described in O'Brien et al. (2003),

Step 2: we calculate the arrival time of the microburst peak in *each* energy channel. We applied the same methodology as in Shumko et al. (2021) by fitting the microburst count time series in each energy channel with a Gaussian superposed with a trend line. As in Shumko et al. (2021), we estimated the goodness of fit using the R^2 statistic. We then visually surveyed the detected microbursts and searched for inverse-dispersed microbursts that were well-fit across multiple energy channels. During this process we discarded microbursts observed when the FIREBIRD-II's collimated detector was affected by dead time or saturation: both are described in Johnson et al. (2020) and in Appendix

A. For each energy channel, we save the time of fitted peak microburst flux, and apply it in the third step.

Step 3: lastly we compare the time differences between the peak microburst flux *across* energies and quantify the dispersion. For this we define the time lag between microburst peak times in each energy channel as $\Delta t_n = t_n - t_0$, where t_n is the peak time of the microburst in the nth energy channel, and t_0 is the peak time in the lowest energy channel. *Inverse* dispersed microbursts have a positive slope with this convention when plotted as a function of energy. Then we quantify the average rate of dispersion by fitting a line to the set of Δt_n. This allows us to readily see dispersion, inverse or otherwise, and calculate the average rate of dispersion in that energy range.

While fitting a line to the Δt_n, we need to consider the instrumental uncertainties in energy and time. One way to do this naturally is with Bayesian inference that defines uncertain parameters using probability density functions (e.g. Kruschke, 2014; Shumko, Johnson, Sample, et al., 2020). It allows us to define the *prior*—the range of possible fit parameter values. The *prior* is then updated during the Bayesian inference, constrained by the data and its uncertainty. The output is an updated version of the *prior*, called the *posterior* distribution.

We parameterize the uncertainty in time using a *likelihood* $\mathcal{L} \sim Normal(\sigma = 18.75)$ with units of [ms]. In energy, we describe the uncertainty with three assumptions: no uncertainty, electrons uniformly distributed within each energy channel range, and electrons exponentially distributed within each energy channel range. While we tested all three assumptions, due to the exponentially-falling microburst energy spectrum (Johnson et al., 2021), the exponential energy channel assumption is the most realistic. For the linear fit *prior* we assumed y-intercept $\sim Normal(\mu = 0, \sigma = 50)$ with units of [ms], and slope $\sim Normal(\mu = 0, \sigma = 5)$ with units [ms/keV].
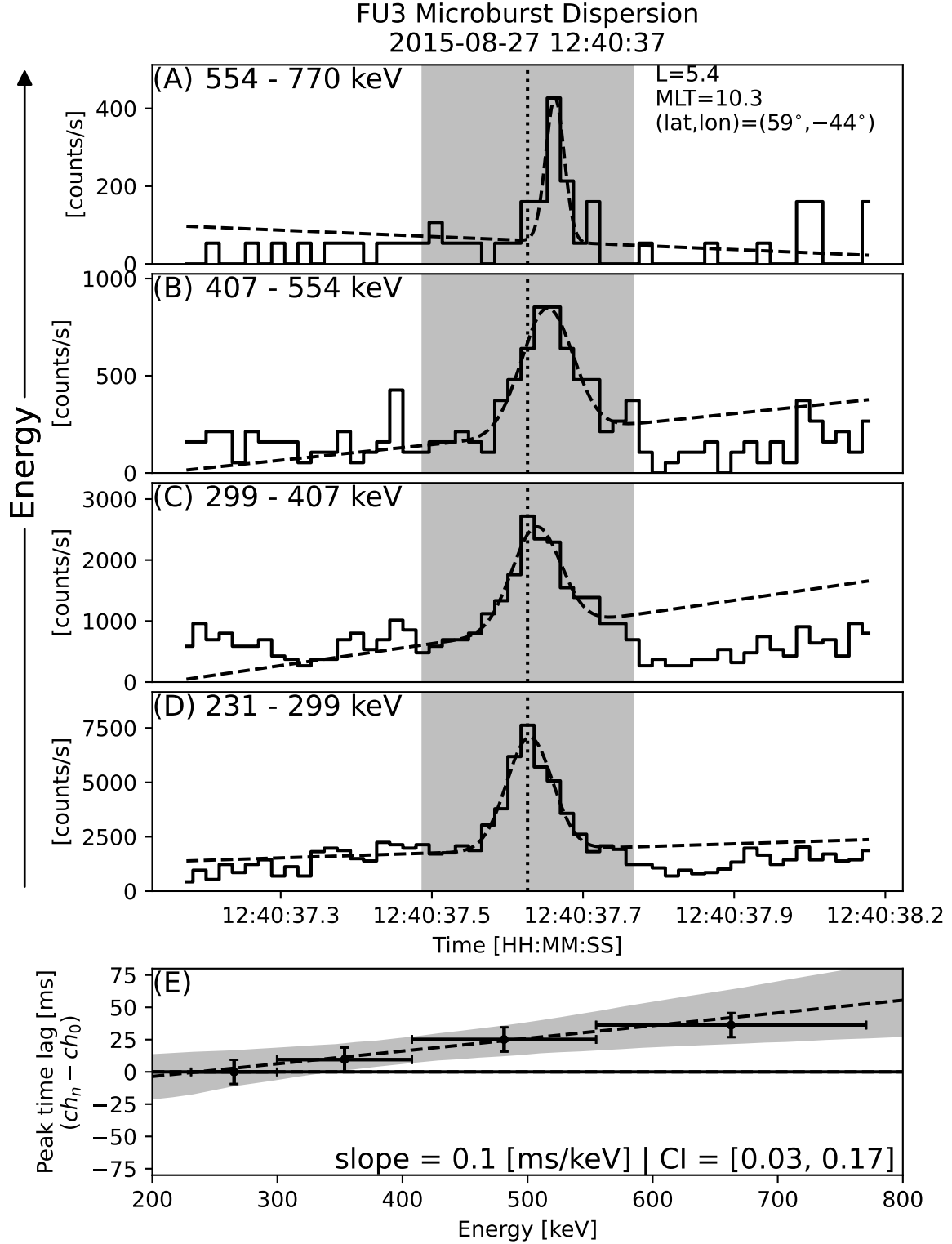
Once fit, we characterize the range of possible slopes and y-intercepts, incorporating the data and uncertainties, with the mean and the 95% credible interval (CI) of the *posterior*. The mean of the *posterior* distribution is similar to the result using traditional least squares optimization.

3 Results

The inverse dispersed microburst of interest here was observed on 27 August 2015 at 12:40:37 UT while FIREBIRD-II Flight Unit 3 (FU3) orbited above the southern tip of Greenland, at an L-shell of 5, and magnetic local time (MLT) of 10. At this location, FU3 only observed electrons that precipitated within a bounce period—inside the region called the bounce loss cone (e.g. J. B. Blake et al., 1996; Shumko et al., 2018; Greeley et al., 2019; Shumko, Johnson, O'Brien, et al., 2020).

Figure 2(A-D) show microburst electron count rates observed in four channels spanning 231-770 keV energies. Superposed on the counts is the result of the automated Gaussian fit with a linear trend (step 2), fit using the interval of data within the vertical grey rectangles. The Gaussian fits converged well to the microburst in these energy channels, with $R^2 > 0.8$. As a guide, we added a vertical dotted black line, aligned to the time of peak counts in the lowest energy channel (panel D), to help visually identify dispersion. The peak microburst counts were delayed at higher energies—the concrete signature of inverse dispersion.

To see this dispersion more clearly, Fig. 2(E) shows the peak time lag, Δt. The x-axis error bars correspond to the energy channel range, estimated with a GEometry ANd Tracking (Geant4; Agostinelli et al., 2003) model of the FIREBIRD-II detectors (Johnson et al., 2020). The y-axis error bars correspond to the 18.75 ms instrument cadence.

Figure 2. Inversely-dispersed microburst observed on 27 August 2015 at 12:40:37 UT. Panels (A)-(D) show the collimated detector counts spanning 230-770 keV energies in descending order. In each panel, FU3's counts are the solid step-line, while the superposition of Gaussian and linear fits is the dashed black line. The grey vertical bars span the 300-ms interval of data used for the fit, and the vertical dotted line is a guide to help identify dispersion. Panel (E) shows the peak time lag as a function of energy. The x-error bars corresponds to the energy channel range and y-errors correspond to the collimated detector cadence. We fit the peak time delay with a linear model. The black dashed line shows the best fit, with the fit slope and the 95% credible interval (CI) annotated.

We then fit the points in Fig. 2(E) with a line to estimate the average dispersion (step 3). As previously mentioned, the uncertainty in peak time is parameterized with a Normal *log-likelihood*, and uncertainty in energy is parameterized with three assumptions and compared. For the exponential energy spectrum uncertainty, we calculated the exponential decay parameter from the data. That is, we fit the microburst flux to

$$J = J_0 e^{-E/E_0},\qquad(2)$$

and we found that the exponential decay parameter to be $E_0 = 86$ keV, similar to the typical microburst spectrum reported by Johnson et al. (2021). Figure 2(E) shows the resulting linear fit, with the optimal TOF dispersion slope of 0.1 [ms/keV] with the 95% credible interval (CI) spanning $0.03-0.17$ [ms/keV]. The other two x-error uncertainty assumptions resulted in a similar optimal dispersion slopes of 0.09 [ms/keV]—a 10% difference.
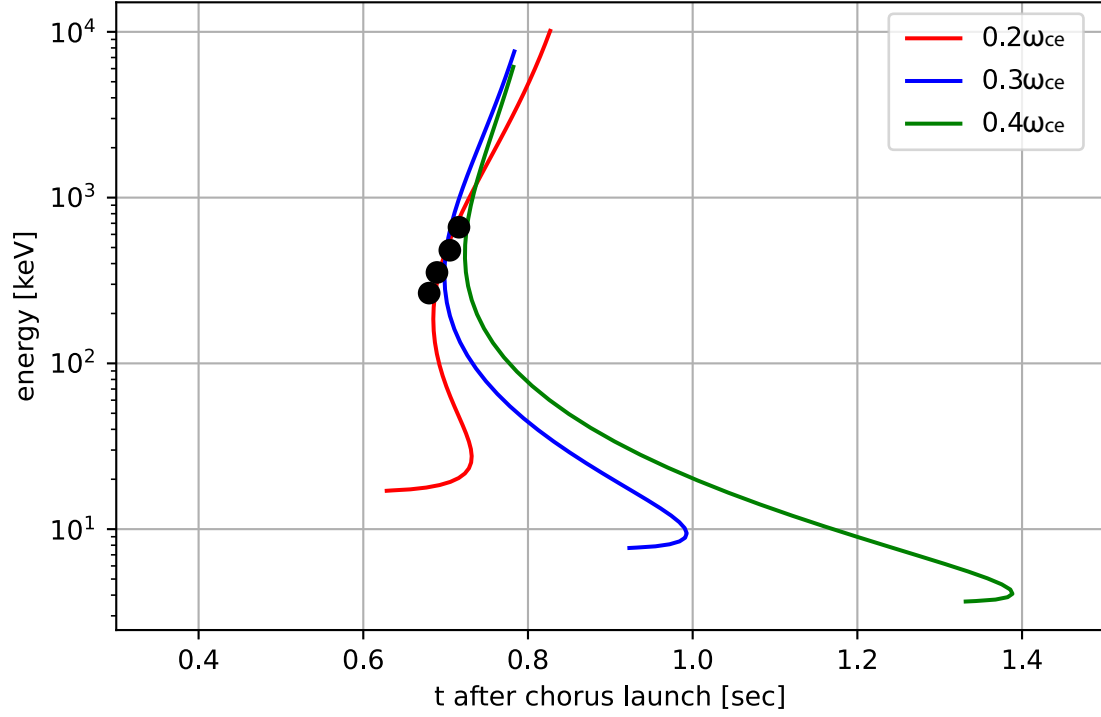
4 Discussion and Conclusion

Notwithstanding a lack of magnetically conjugate high-altitude satellites at this time, we compared the rate of dispersion delay to the TOF model (Miyoshi et al., 2010; Saito et al., 2012) with the following inputs. A 3 kHz/s rising tone chorus element sweep rate, and plasma density estimated using the Sheeley et al. (2001) model evaluated at the L-shell of FU3. We assume the constant plasma density along the field line. Figure 3 shows three resulting TOF curves corresponding to different chorus wave frequencies spanning $0.2 - 0.4$ ω_{ce}. Our observation is consistent with the 0.2 ω_{ce} curve—significantly constraining the wave frequency that generated the microburst.

This conclusion is observationally supported by the Shue et al. (2019) and Shumko et al. (2021) results. The authors found that the chorus rising tone frequency sweeps over a wide range of frequencies on timescales longer than relativistic microbursts by a factor of 3-4. Since microburst electrons are scattered over a duration shorter than the frequency sweep, this suggests that relativistic microbursts are scattered by a relatively narrower band of wave frequency.

In modeling this microburst, we assumed that the plasma density is uniform along the magnetic field line (Sheeley et al., 2001). In reality, this assumption is simplistic as modulations in the plasma density can be as small as a few tens of km (Agapitov et al., 2011; Hosseini et al., 2021). This scale is similar to the ~ 28 km equatorial distance that FU3 traversed during this microburst (estimated using the Tsyganenko (1989) magnetic field model). Density irregularities can duct chorus waves to high magnetic latitudes without significant attenuation, and modify the ratio of the plasma to cyclotron frequencies that controls the resonant energies involved in wave-particle interactions (Summers et al., 1998; Thorne et al., 2005; Miyoshi et al., 2015; Chen et al., 2022; A. V. Artemyev et al., 2021). A parametric study of this effect on the electron TOF will be a subject of future work.

Inverse dispersed microburst observations have also been reported by Kawamura et al. (2021), who analyzed a FIREBIRD-II conjunction above an auroral all sky imager that concurrently observed pulsating aurora. The authors detected the inverse TOF energy dispersion by applying the Hilbert transform and reported that the Δt were shorter than the FIREBIRD-II cadence during that observation.

Besides Kawamura et al. (2021) and this study, inverse dispersed microbursts are absent in the literature. Despite our efforts to automate this methodology to find more inverse dispersed microbursts, the FIREBIRD-II collimated detector is sometimes affected by dead time and saturation that can appear as inversely dispersed microbursts. The example in Appendix A demonstrates this saturation characteristic. As a result, reliable identification of inverse dispersed microbursts observed by FIREBIRD-II must be done by visual inspection.

Figure 3. Time-of-flight curves derived from the Miyoshi-Saito model (Saito et al., 2012). The colored curves correspond to chorus waves with normalized frequencies spanning $0.2 - 0.4 \, \omega_{ce}$. The four points correspond to the observed dispersion with the highest energy point pinned to the time nearest to where the curves intersect.

While FIREBIRD-II's 12.5−18.75 ms cadence, and 6 energy channels appear sufficient for observing microburst dispersion, working with this data taught us a few lessons for future instrument development. For an instrument designed to test the TOF model (Saito et al., 2012; Miyoshi et al., 2010), especially to observe the dispersion inflection in the TOF curves (at 200 keV in Fig. 3) the overarching requirement is to observe enough electrons across an energy range spanning 10s keV - 1 MeV. This is where the main difficulty lies—there are exponentially fewer high-energy electrons than low-energy electrons, and the required fast sample rate necessitates the use of a large geometric factor for detection of high energy flux (e.g. Sullivan, 1971). This requirement must be met under the constraints of sampling quickly enough, with enough differential energy channels, and over a sufficient energy span. The number of differential energy channels may also be crucial to constrain the wave generation region via ray tracing models.

Moreover, there may be a physical explanation for why inverse-dispersed microbursts are seldom observed. While the microburst studied here precipitated immediately as it was in the bounce loss cone region in the North Atlantic, this is not always the case. If the microburst is observed in the drift loss cone, some of the microburst electrons may survive successive glances off the atmosphere, shown by J. B. Blake et al. (1996) and Shumko et al. (2018), and any signature of inverse TOF dispersion will be quickly undone by bounce-phase mixing and drift (O'Brien et al., 2022).

In summary, we found a clear inverse dispersed microburst where the high energy electrons lagged behind the low energy electrons in the 231-770 keV range. We estimated that the higher energy electrons arrived progressively later with a TOF dispersion of 0.1 [ms/keV]. Considering the instrument uncertainty, the range of probable dispersion values spans 0.03−0.17 [ms/keV]. This counter-intuitive effect is theoretically supported, assuming a field-aligned 0.2 ω_{ce} chorus wave resonated with electrons via the $n = 1$ cyclotron resonance (Miyoshi et al., 2010; Saito et al., 2012). Consequently, our observation supports that the first-order cyclotron resonance was most efficient, and the chorus wave propagated to high magnetic latitudes without significant attenuation (Thorne et al., 2005; W. Li et al., 2011; Agapitov et al., 2013; Colpitts et al., 2020; Chen et al., 2022). It is also evidence that a single microburst can be attributed to scattering by a wave with a narrow range of frequencies. Finally, this study confirms that the TOF theory produces credible results, and helps constrain the high-altitude plasma and wave environment where microbursts are generated.

Appendix A Saturation and Dead Time

The FIREBIRD-II count data is at times affected by dead time and saturation. Identifying dead time is relatively straightforward as additional penetrating particles do not produce a signal, resulting in 0 counts in the HiRes data across all energy channels.

FIREBIRD-II detectors also saturate when the electron energy spectrum is hard (Johnson et al., 2020). This is a result of how the Dual Amplifier Pulse Peak Energy Rundown (DAPPER) integrated circuit (J. Blake et al., 2016) digitizes the accumulated charge. The charge pulse is digitized by creating a fixed-voltage, variable duration digital pulse with the pulse duration linearly proportional to the input from the detector. Therefore, higher energy electrons take longer to process; during which no other electrons are counted. When enough high-energy electrons are present, the amount of lower energy electrons is undercounted. As a result, lower energy channel counts sag as the higher energy channels peak. Johnson et al. (2020) describes this saturation in more detail and provides an example in their Fig. 8.

This saturation results in microbursts that appear dispersed, so they must be visually inspected. Figure A1 demonstrates this saturation. It shows a very intense microburst, spanning the full energy range of the instrument. The two lowest energy chan-

nel counts in Panels (E) and (F) sag around 26.3 seconds—right as the > 1 MeV channel counts in Panel (A) peak. This is the tell-tale sign of saturation. Soon after, as $>$ 1 MeV counts decrease, the counts in Panels (E) and (F) rebound. As a result, for the lowest energy channels, the automated Gaussian fitting algorithm converged at the pre-saturated microburst peak, resulting in an artificial (and compelling) inverse dispersion. For this reason, we urge researchers to carefully inspect each microburst for saturation before embarking on a statistical study of microburst dispersion.
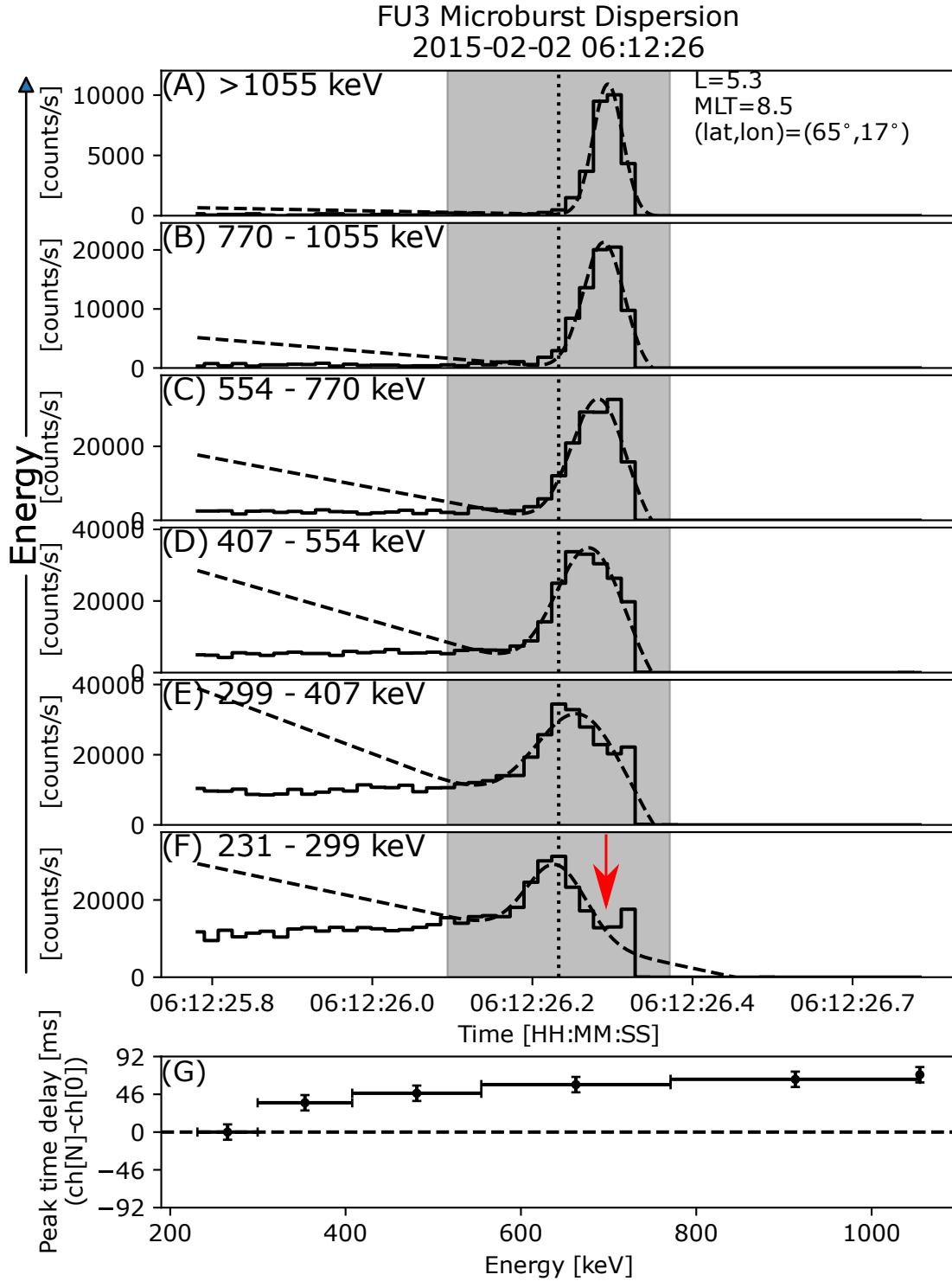
Appendix B Open Research

The FIREBIRD-II data is available online at `https://solar.physics.montana.edu/FIREBIRD_II/`. The authors used the pymc3 Python package (Salvatier et al., 2016) version 3.11.5 to implement the Bayesian fit. The code to reproduce these results is available on GitHub: `https://github.com/mshumko/microburst_dispersion`, and is archived on Zenodo: `https://doi.org/10.5281/zenodo.7799828/`.

References

Agapitov, O., Artemyev, A., Krasnoselskikh, V., Khotyaintsev, Y. V., Mourenas, D., Breuillard, H., ... Rolland, G. (2013). Statistics of whistler mode waves in the outer radiation belt: Cluster staff-sa measurements. *Journal of Geophysical Research: Space Physics*, *118*(6), 3407–3420.

Agapitov, O., Krasnoselskikh, V., Dudok de Wit, T., Khotyaintsev, Y., Pickett, J. S., Santolik, O., & Rolland, G. (2011). Multispacecraft observations of chorus emissions as a tool for the plasma density fluctuations' remote sensing. *Journal of Geophysical Research: Space Physics*, *116*(A9), n/a–n/a. Retrieved from `http://dx.doi.org/10.1029/2011JA016540` (A09222) doi: 10.1029/2011JA016540

Agapitov, O., Mourenas, D., Artemyev, A., Mozer, F., Hospodarsky, G., Bonnell, J., & Krasnoselskikh, V. (2018). Synthetic empirical chorus wave model from combined van allen probes and cluster statistics. *Journal of Geophysical Research: Space Physics*, *123*(1), 297–314.

Agostinelli, S., Allison, J., Amako, K. a., Apostolakis, J., Araujo, H., Arce, P., ... others (2003). Geant4—a simulation toolkit. *Nuclear instruments and methods in physics research section A: Accelerators, Spectrometers, Detectors and Associated Equipment*, *506*(3), 250–303.

Artemyev, A., Agapitov, O., Mourenas, D., Krasnoselskikh, V., Shastun, V., & Mozer, F. (2016). Oblique whistler-mode waves in the earth's inner magnetosphere: Energy distribution, origins, and role in radiation belt dynamics. *Space Science Reviews*, *200*, 261–355.

Artemyev, A., Zhang, X.-J., Zou, Y., Mourenas, D., Angelopoulos, V., Vainchtein, D., ... Wilkins, C. (2022). On the nature of intense sub-relativistic electron precipitation. *Journal of Geophysical Research: Space Physics*, *127*(6), e2022JA030571.

Artemyev, A. V., Demekhov, A., Zhang, X.-J., Angelopoulos, V., Mourenas, D., Fedorenko, Y. V., ... others (2021). Role of ducting in relativistic electron loss by whistler-mode wave scattering. *Journal of Geophysical Research: Space*

Figure A1. A microburst that erroneously appears inverse dispersed due to saturation. Counts in the two lowest energy channels, shown in panels (E) and (F), sag right as the > 1 MeV channel counts, shown in panel (A) peaks around 06:12:26.3. This leads to an erroneous signature of inverse dispersion.

Physics, *126*(11), e2021JA029851.

Blake, J., Mauk, B., Baker, D., Carranza, P., Clemmons, J., Craft, J., . . . others (2016). The fly's eye energetic particle spectrometer (feeps) sensors for the magnetospheric multiscale (mms) mission. *Space Science Reviews*, *199*, 309–329.

Blake, J. B., Looper, M. D., Baker, D. N., Nakamura, R., Klecker, B., & Hovestadt, D. (1996). New high temporal and spatial resolution measurements by sampex of the precipitation of relativistic electrons. *Advances in Space Research*, *18*(8), 171 - 186. Retrieved from `http://www.sciencedirect.com/science/article/pii/0273117795009698` doi: http://dx.doi.org/10.1016/0273-1177(95)00969-8

Bortnik, J., & Thorne, R. (2007). The dual role of elf/vlf chorus waves in the acceleration and precipitation of radiation belt electrons. *Journal of Atmospheric and Solar-Terrestrial Physics*, *69*(3), 378–386.

Breneman, A., Crew, A., Sample, J., Klumpar, D., Johnson, A., Agapitov, O., . . . others (2017). Observations directly linking relativistic electron microbursts to whistler mode chorus: Van allen probes and FIREBIRD II. *Geophysical Research Letters*.

Capannolo, L., Li, W., Ma, Q., Chen, L., Shen, X.-C., Spence, H., . . . others (2019). Direct observation of subrelativistic electron precipitation potentially driven by emic waves. *Geophysical Research Letters*, *46*(22), 12711–12721.

Chen, L., Breneman, A. W., Xia, Z., & Zhang, X.-j. (2020). Modeling of bouncing electron microbursts induced by ducted chorus waves. *Geophysical Research Letters*, *47*(17), e2020GL089400. Retrieved from `https://agupubs.onlinelibrary.wiley.com/doi/abs/10.1029/2020GL089400` (e2020GL089400 10.1029/2020GL089400) doi: https://doi.org/10.1029/2020GL089400

Chen, L., Zhang, X.-J., Artemyev, A., Angelopoulos, V., Tsai, E., Wilkins, C., & Horne, R. B. (2022). Ducted chorus waves cause sub-relativistic and relativistic electron microbursts. *Geophysical Research Letters*, *49*(5), e2021GL097559.

Colpitts, C., Miyoshi, Y., Kasahara, Y., Delzanno, G. L., Wygant, J. R., Cattell, C. A., . . . others (2020). First direct observations of propagation of discrete chorus elements from the equatorial source to higher latitudes, using the van allen probes and arase satellites. *Journal of Geophysical Research: Space Physics*, *125*(10), e2020JA028315.

Crew, A. B., Spence, H. E., Blake, J. B., Klumpar, D. M., Larsen, B. A., O'Brien, T. P., . . . Widholm, M. (2016). First multipoint in situ observations of electron microbursts: Initial results from the NSF FIREBIRD II mission. *Journal of Geophysical Research: Space Physics*, *121*(6), 5272–5283. Retrieved from `http://dx.doi.org/10.1002/2016JA022485` (2016JA022485) doi: 10.1002/2016JA022485

Douma, E., Rodger, C. J., Blum, L. W., & Clilverd, M. A. (2017). Occurrence characteristics of relativistic electron microbursts from SAMPEX observations. *Journal of Geophysical Research: Space Physics*, *122*(8), 8096–8107. Retrieved from `http://dx.doi.org/10.1002/2017JA024067` (2017JA024067) doi: 10.1002/2017JA024067

Duderstadt, K. A., Huang, C.-L., Spence, H. E., Smith, S., Blake, J. B., Crew, A. B., . . . Vitt, F. M. (2021). Estimating the impacts of radiation belt electrons on atmospheric chemistry using firebird ii and van allen probes observations. *Journal of Geophysical Research: Atmospheres*, *n/a*(n/a), e2020JD033098. Retrieved from `https://agupubs.onlinelibrary.wiley.com/doi/abs/10.1029/2020JD033098` (e2020JD033098 2020JD033098) doi: https://doi.org/10.1029/2020JD033098

Greeley, A., Kanekal, S., Baker, D., Klecker, B., & Schiller, Q. (2019). Quantifying the contribution of microbursts to global electron loss in the radiation belts.

Journal of Geophysical Research: Space Physics.

Horne, R. B., & Thorne, R. M. (2003). Relativistic electron acceleration and precipitation during resonant interactions with whistler-mode chorus. *Geophysical Research Letters*, *30*(10). Retrieved from http://dx.doi.org/10.1029/2003GL016973 (1527) doi: 10.1029/2003GL016973

Hosseini, P., Agapitov, O., Harid, V., & Gołkowski, M. (2021). Evidence of small scale plasma irregularity effects on whistler mode chorus propagation. *Geophysical Research Letters*, *48*(5), e2021GL092850.

Johnson, A., Shumko, M., Griffith, B., Klumpar, D., Sample, J., Springer, L., . . . others (2020). The FIREBIRD-II CubeSat mission: Focused investigations of relativistic electron burst intensity, range, and dynamics. *Review of Scientific Instruments*, *91*(3), 034503.

Johnson, A., Shumko, M., Sample, J., Griffith, B., Klumpar, D., Spence, H., & Blake, J. B. (2021). The energy spectra of electron microbursts between 200 kev and 1 mev. *Journal of Geophysical Research: Space Physics*, *126*(11), e2021JA029709.

Kang, N., Bortnik, J., Zhang, X., Claudepierre, S., & Shi, X. (2022). Relativistic microburst scale size induced by a single point-source chorus element. *Geophysical Research Letters*, *49*(23), e2022GL100841.

Kawamura, M., Sakanoi, T., Fukizawa, M., Miyoshi, Y., Hosokawa, K., Tsuchiya, F., . . . others (2021). Simultaneous pulsating aurora and microburst observations with ground-based fast auroral imagers and cubesat firebird-ii. *Geophysical Research Letters*, *48*(18), e2021GL094494.

Kruschke, J. (2014). Doing bayesian data analysis: A tutorial with r, jags, and stan.

Lejosne, S., Allison, H. J., Blum, L. W., Drozdov, A. Y., Hartinger, M. D., Hudson, M. K., . . . Zhao, H. (2022). Differentiating between the leading processes for electron radiation belt acceleration. *Frontiers in Astronomy and Space Sciences*, 144.

Li, J., Bortnik, J., An, X., Li, W., Angelopoulos, V., Thorne, R. M., . . . others (2019). Origin of two-band chorus in the radiation belt of earth. *Nature communications*, *10*(1), 4672.

Li, W., Bortnik, J., Thorne, R., & Angelopoulos, V. (2011). Global distribution of wave amplitudes and wave normal angles of chorus waves using themis wave observations. *Journal of Geophysical Research: Space Physics*, *116*(A12).

Lorentzen, K. R., Blake, J. B., Inan, U. S., & Bortnik, J. (2001). Observations of relativistic electron microbursts in association with VLF chorus. *Journal of Geophysical Research: Space Physics*, *106*(A4), 6017–6027. Retrieved from http://dx.doi.org/10.1029/2000JA003018 doi: 10.1029/2000JA003018

Miyoshi, Y., Kataoka, R., Kasahara, Y., Kumamoto, A., Nagai, T., & Thomsen, M. (2013). High-speed solar wind with southward interplanetary magnetic field causes relativistic electron flux enhancement of the outer radiation belt via enhanced condition of whistler waves. *Geophysical Research Letters*, *40*(17), 4520–4525.

Miyoshi, Y., Katoh, Y., Nishiyama, T., Sakanoi, T., Asamura, K., & Hirahara, M. (2010). Time of flight analysis of pulsating aurora electrons, considering wave-particle interactions with propagating whistler mode waves. *Journal of Geophysical Research: Space Physics*, *115*(A10).

Miyoshi, Y., Morioka, A., Misawa, H., Obara, T., Nagai, T., & Kasahara, Y. (2003). Rebuilding process of the outer radiation belt during the 3 november 1993 magnetic storm: Noaa and exos-d observations. *Journal of Geophysical Research: Space Physics*, *108*(A1), SMP–3.

Miyoshi, Y., Oyama, S., Saito, S., Kurita, S., Fujiwara, H., Kataoka, R., . . . others (2015). Energetic electron precipitation associated with pulsating aurora: Eiscat and van allen probe observations. *Journal of Geophysical Research: Space Physics*, *120*(4), 2754–2766.

Miyoshi, Y., Saito, S., Kurita, S., Asamura, K., Hosokawa, K., Sakanoi, T., ... others (2020). Relativistic electron microbursts as high energy tail of pulsating aurora electrons.

O'Brien, T. P., Lorentzen, K. R., Mann, I. R., Meredith, N. P., Blake, J. B., Fennell, J. F., ... Anderson, R. R. (2003). Energization of relativistic electrons in the presence of ULF power and MeV microbursts: Evidence for dual ULF and VLF acceleration. *Journal of Geophysical Research: Space Physics*, *108*(A8). Retrieved from http://dx.doi.org/10.1029/2002JA009784 doi: 10.1029/2002JA009784

Omura, Y., Hikishima, M., Katoh, Y., Summers, D., & Yagitani, S. (2009). Nonlinear mechanisms of lower-band and upper-band vlf chorus emissions in the magnetosphere. *Journal of Geophysical Research: Space Physics*, *114*(A7).

O'Brien, T. P., Lemon, C., & Blake, J. B. (2022). Electron precipitation curtains—simulating the microburst origin hypothesis. *Journal of Geophysical Research: Space Physics*, *127*(8), e2022JA030370.

Reeves, G., Spence, H. E., Henderson, M., Morley, S., Friedel, R., Funsten, H., ... others (2013). Electron acceleration in the heart of the van allen radiation belts. *Science*, *341*(6149), 991–994.

Saito, S., Miyoshi, Y., & Seki, K. (2012). Relativistic electron microbursts associated with whistler chorus rising tone elements: Gemsis-rbw simulations. *Journal of Geophysical Research: Space Physics*, *117*(A10), n/a–n/a. Retrieved from http://dx.doi.org/10.1029/2012JA018020 (A10206) doi: 10.1029/2012JA018020

Salvatier, J., Wiecki, T. V., & Fonnesbeck, C. (2016, apr). Probabilistic programming in python using PyMC3. *PeerJ Computer Science*, *2*, e55. Retrieved from https://doi.org/10.7717/peerj-cs.55 doi: 10.7717/peerj-cs.55

Sato, N., Wright, D., Carlson, C., Ebihara, Y., Sato, M., Saemundsson, T., ... Lester, M. (2004). Generation region of pulsating aurora obtained simultaneously by the fast satellite and a syowa-iceland conjugate pair of observatories. *Journal of Geophysical Research: Space Physics*, *109*(A10).

Sheeley, B., Moldwin, M., Rassoul, H., & Anderson, R. (2001). An empirical plasmasphere and trough density model: Crres observations. *Journal of Geophysical Research: Space Physics*, *106*(A11), 25631–25641.

Shen, Y., Chen, L., Zhang, X.-J., Artemyev, A., Angelopoulos, V., Cully, C. M., ... others (2021). Conjugate observation of magnetospheric chorus propagating to the ionosphere by ducting. *Geophysical Research Letters*, *48*(23), e2021GL095933.

Shue, J.-H., Nariyuki, Y., Katoh, Y., Saito, S., Kasahara, Y., Hsieh, Y.-K., ... Goto, Y. (2019). A systematic study in characteristics of lower band rising-tone chorus elements. *Journal of Geophysical Research: Space Physics*, *124*(11), 9003–9016.

Shumko, M., Blum, L. W., & Crew, A. B. (2021). Duration of individual relativistic electron microbursts: A probe into their scattering mechanism. *Geophysical Research Letters*, *48*(17), e2021GL093879.

Shumko, M., Johnson, A., Sample, J., Griffith, B. A., Turner, D. L., O'Brien, T. P., ... Claudepierre, S. G. (2020). Electron microburst size distribution derived with AeroCube-6. *Journal of Geophysical Research: Space Physics*, e2019JA027651.

Shumko, M., Johnson, A. T., O'Brien, T. P., Turner, D. L., Greeley, A. D., Sample, J. G., ... Halford, A. J. (2020). Statistical properties of electron curtain precipitation estimated with aerocube-6. *Journal of Geophysical Research: Space Physics*, *125*(12), e2020JA028462. Retrieved from https://agupubs.onlinelibrary.wiley.com/doi/abs/10.1029/2020JA028462 (e2020JA028462 10.1029/2020JA028462) doi: https://doi.org/10.1029/2020JA028462

Shumko, M., Sample, J., Johnson, A., Blake, B., Crew, A., Spence, H., ... Handley, M. (2018). Microburst scale size derived from multiple bounces of a microburst simultaneously observed with the firebird-ii cubesats. *Geophysical Research Letters*, *45*(17), 8811-8818. Retrieved from https://agupubs.onlinelibrary.wiley.com/doi/abs/10.1029/2018GL078925 doi: 10.1029/2018GL078925

Sullivan, J. (1971). Geometric factor and directional response of single and multi-element particle telescopes. *Nuclear Instruments and methods*, *95*(1), 5–11.

Summers, D., Thorne, R. M., & Xiao, F. (1998). Relativistic theory of wave-particle resonant diffusion with application to electron acceleration in the magnetosphere. *Journal of Geophysical Research: Space Physics*, *103*(A9), 20487–20500.

Thorne, R. M., O'Brien, T. P., Shprits, Y. Y., Summers, D., & Horne, R. B. (2005). Timescale for MeV electron microburst loss during geomagnetic storms. *Journal of Geophysical Research: Space Physics*, *110*(A9). Retrieved from http://dx.doi.org/10.1029/2004JA010882 (A09202) doi: 10.1029/2004JA010882

Tsurutani, B. T., & Lakhina, G. S. (1997). Some basic concepts of wave-particle interactions in collisionless plasmas. *Reviews of Geophysics*, *35*(4), 491–501.

Tsyganenko, N. (1989). A solution of the chapman-ferraro problem for an ellipsoidal magnetopause. *Planetary and Space Science*, *37*(9), 1037 - 1046. Retrieved from http://www.sciencedirect.com/science/article/pii/0032063389900767 doi: http://dx.doi.org/10.1016/0032-0633(89)90076-7

Walker, A. D. M. (1993). *Plasma waves in the magnetosphere* (Vol. 24). Springer Science & Business Media.

Yau, A. W., Whalen, B. A., & McEwen, D. (1981). Rocket-borne measurements of particle pulsation in pulsating aurora. *Journal of Geophysical Research: Space Physics*, *86*(A7), 5673–5681.